Global and Planetary Change 243 (2024) 104613

Contents lists available at ScienceDirect

Global and Planetary Change

journal homepage: www.elsevier.com/locate/gloplacha

Contrasting orbital rhythms preserved in loess grain-size records across the Chinese Loess Plateau

Deai Zhao [a], Guoqiao Xiao [b,*], Chunju Huang [a], Haibin Wu [c,d], Qingzhen Hao [c,d], David B. Kemp [a], Shaohua Tian [a], Zhipeng Wu [c,e], Hao Lu [e], Gaowen Dai [a], Shuzhen Peng [f], Changyan Tang [g], Jianyu Wu [c,d], Yating Lin [c,d], Shuya Zhu [c,d], Qiuzhen Yin [e]

[a] State Key Laboratory of Biogeology and Environmental Geology and Hubei Key Laboratory of Critical Zone Evolution, School of Earth Sciences, China University of Geosciences, Wuhan 430074, China
[b] Hubei Key Laboratory of Critical Zone Evolution, School of Geography and Information Engineering, China University of Geosciences, Wuhan 430078, China
[c] Key Laboratory of Cenozoic Geology and Environment, Institute of Geology and Geophysics, Chinese Academy of Sciences, Beijing 100029, China
[d] University of Chinese Academy of Sciences, Beijing 100049, China
[e] Earth and Climate Research Center, Earth and Life Institute, Universite catholique de Louvain, Louvain-la-Neuve 1348, Belgium
[f] School of Tourism, Resources and Environment, Taishan University, Tai'an 271021, China
[g] Key Lab of Submarine Geosciences and Prospecting Techniques, MOE, Ocean University of China, Qingdao 266100, China

ARTICLE INFO

Editor: Dr. Sun Jimin

Keywords:
Loess
East Asia Winter monsoon
Quaternary
Grain size
Precession
Ice-age cycle

ABSTRACT

The loess-paleosol sequences on the Chinese Loess Plateau (CLP) are among the best terrestrial archives for recording orbital-scale global paleoenvironmental and East Asian monsoon changes during the Quaternary Period. Dust provenance and climate patterns vary across the CLP due to its vast size. However, whether available climate proxies were influenced by varying signals from the different dust source areas remains unknown. Here we present time series analysis results of high-resolution grain-size records from four loess sections (Jingbian, Xifeng, Baoji, and Weinan sections) spanning a north to south transect in the eastern CLP across the past 0.7 Ma. By comparison with data from the previously reported Luochuan section in the eastern CLP, and the Gulang, Menyuan, Jingyuan, Lanzhou, and Linxia sections in the western CLP, it is revealed that the dominant orbital signal in grain size variations in the eastern CLP is the ~100-kyr ice-age cycle, with precession only very weakly expressed. By contrast, western CLP records exhibit both ~100-kyr and ~ 20-kyr precession cycles. We show that this contrasting orbital patterns between the eastern and western CLP are likely to be influenced by the climate signals from the respective source regions. We 2propose that the grain size variations in the western CLP not only contain the ~100-kyr ice-age related winter monsoon cycles but also precession cycles related to the mid-latitude Westerlies and the Tibetan Plateau. The grain size variations in the eastern CLP are, by contrast, mainly influenced by ~100-kyr ice-age cycle-regulated winter monsoon changes. The spatial diversity of periodicity in loess grain-size records from the CLP suggests that caution should be taken when discussing the periodicities of loess records based on any single site.

1. Introduction

The thick loess-paleosol deposits of the CLP preserve some of the best archives of Quaternary climate change, comparable in both fidelity and utility to those obtainable from deep-sea sediments and polar ice cores (Liu, 1985; Liu and Ding, 1998). The accumulation processes of loess are influenced by glacial and interglacial climate fluctuations (An et al., 1990; Liu and Ding, 1998). During glacial intervals, the climate over the CLP was cold and dry, leading to the formation of loess units, whereas during interglacial intervals the climate was warm and moist, resulting in the formation of paleosol units. In addition, because the CLP is situated within the East Asian monsoon region, the formation of loess is significantly affected by the winter and summer monsoons (An et al., 1990; Guo et al., 2002). Specifically, the delivery of dust from the arid regions of the Asian interior occurs via the East Asian winter monsoon and Westerlies, and the development of paleosols is facilitated by

* Corresponding author at: Hubei Key Laboratory of Critical Zone Evolution, School of Geography and Information Engineering, China University of Geosciences, Wuhan 430078, China.
E-mail addresses: gqxiaocug@126.com, xgqiaocug@gmail.com (G. Xiao).

https://doi.org/10.1016/j.gloplacha.2024.104613
Received 10 August 2024; Received in revised form 12 October 2024; Accepted 20 October 2024
Available online 22 October 2024

moisture delivered via the East Asian summer monsoon (Lu et al., 2022). Detailed stratigraphic correlation across the CLP has shown that the loess and paleosol units of Chinese loess contain comparable spatial features (Ding et al., 2002; Sun et al., 2021). Spectral analysis indicates that ~100 ka, ~40 ka, and ~ 20 ka orbital periodicities can be well-preserved in loess-paleosol sequences of the CLP, as well as the well-known and significant mid-Pleistocene transition at ~0.85 Ma, when the dominant forcing switched from 41-kyr to ~100-kyr period cycles (Ding et al., 1994; Guo et al., 2000, 2005; Lu et al., 2004b; Sun et al., 2006, 2019). Thus, some classical loess-paleosol sections on the CLP, such as Luochuan, Xifeng, Baoji, Weinan, and Jingbian (Fig. 1b), are well-known as representative sections for recording the evolution of the mid-latitudinal East Asian monsoon during the Quaternary (Beck et al., 2018; Ding et al., 2002, 2005; Liu, 1985; Zhou et al., 2023).

Despite these advances, recent studies have revealed that the cyclic variations recorded at different loess sections are not identical. For example, for the last interglacial paleosol unit S1 across the CLP, the magnetic susceptibility record — a summer monsoon proxy — shows three distinct precession cycles in some sections, but merely a single peak in the rest (Ma et al., 2017). Some researchers attributed this phenomenon to differences in sedimentation rate and pedogenesis (Guo et al., 2022; Ma et al., 2017). Indeed, it is correct that sedimentation rates across the CLP varied significantly, with rates in the northwest CLP 2 to 3 times higher than those in the southeast CLP due to its proximity to source areas. This may mean that some sections with low sedimentation rates cannot record precession cycles (Ma et al., 2017). At the same time, there are significant differences in precipitation across the CLP (Fig. 1), with the rainfall in the northwest CLP being less than 200 mm, and up to 650 mm in the southeast CLP. Low precipitation may make summer monsoon proxies in loess (such as magnetic susceptibility) less sensitive to changes in rainfall due to the weaker pedogenesis it causes (Guo et al., 2022). In the southeast CLP, high precipitation and low sedimentation rates could lead to the merging of multiple sub-paleosol layers and thus an eventual absence of precession-scale variability (Ma et al., 2017). However, recently reported free iron/total iron ratio data (a summer monsoon proxy) in the Madang loess section in the lower latitude (~30°N) monsoon region exhibits clear ~20-kyr precession cycles (Li et al., 2024), whereas this proxy obtained from the CLP (34–37°N) shows dominant ~100-kyr cycles (Guo et al., 2000, 2005), suggesting that geographic differences in climate played an important role in controlling the diversity of orbital responses to the same summer monsoon proxy.

Geographic differences in climate and sedimentation rates across the CLP can not only lead to the differences in recorded orbital responses in summer monsoon proxies, but also in winter monsoon proxies. Previous studies for sections in the western CLP (west of the Liupan Mountains), such as the Gulang, Jingyuan, Linxia, Xining, Menyuan and Xinzhuangyuan sections, revealed that grain size — a winter monsoon proxy — in the last interglacial paleosol unit S1 exhibits more distinct precession cycles than in sections from the eastern CLP (Lu et al., 2004a; Ma et al., 2017; Xiao et al., 2023; Yang and Ding, 2014). The absence of precession cycles in the grain-size record of the S1 unit from the eastern CLP was attributed to reduced sedimentation rate and a merging of sub-paleosol layers due to strong chemical weathering (Ma et al., 2017). However, the S1 unit in sections with high sedimentation rates and weak weathering from the north part of the eastern CLP, such as at the Jingbian, Yulin, Jiyuan and Hongde sections, also lacks precession in the grain-size records (Ding et al., 2005; Yang and Ding, 2014). This suggests that other factors may be responsible for the inconsistency in the orbital character of loess grain-size records. Dust supply varies across the CLP (Xiao et al., 2012; Zhang et al., 2021; Zhou et al., 2022), and thus one possibility is that the periodicity recorded in loess grain-size data may be influenced by the climate signals of source areas (Xiao et al., 2023).

To test whether differences in dust supply influence the periodicity encoded in grain-size records across the CLP, we obtained high-resolution grain-size data spanning the past 0.7 Ma from the Jingbian section in the northern part of the CLP, the Xifeng section in the central part of the CLP, and the Baoji and Weinan sections in the southern part of the eastern CLP. By comparing our data with those from the previously reported Luochuan and Dingbian sections in the eastern CLP, as well as the Gulang, Menyuan, Jingyuan, Lanzhou, and Linxia sections in the western CLP, we provide a comprehensive assessment of the possible factors that influenced the recoding of orbital-scale variations in loess grain size across the CLP.

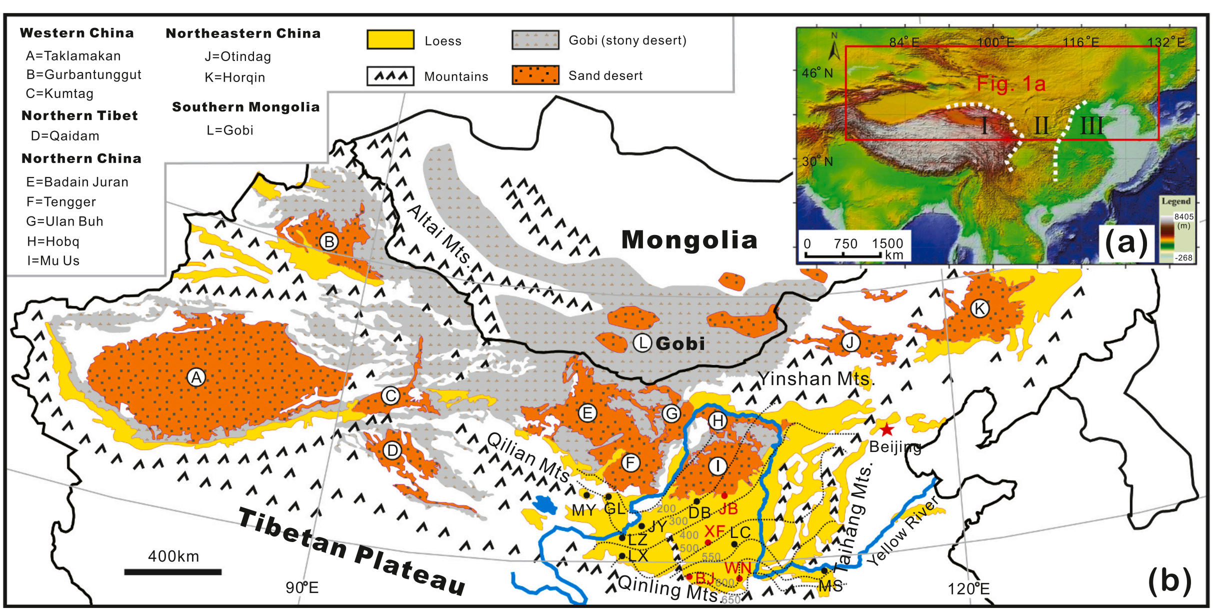

Fig. 1. Landforms of East Asia (a) and location of the Chinese Loess Plateau (b) and its potential desert source areas (modified after Xiao et al., 2012). The red and black dots show the studied loess sections and published sections mentioned in the text, respectively. MY, Menyuan; GL, Gulang; LZ, Lanzhou; LX, Linxia; JY, Jingyuan; DB, Dingbian; JB, Jingbian; XF, Xifeng; LC, Luochuan; BJ, Baoji; WN, Weinan; MS, Mangshan. Black dashed lines represent modern mean annual precipitation isopleth. Black Roman numerals denote the three major terraces of China. (For interpretation of the references to colour in this figure legend, the reader is referred to the web version of this article.)

2. Materials and methods

2.1. Geological setting and studied sections

The landform of China can be broadly divided into three major terraces (Fig. 1a), and the CLP is located on the second terrace. The CLP is bounded by the Riyueshan Mountains to the west, the Taihang Mountains to the east, the Qinling Mountains to the south, and the Great Wall to the north. The CLP is over 1000 km in length from east to west, and over 500 km in width from north to south, with an area of approximately 440,000 km^2 (Liu, 1985). Traditionally, the CLP is divided into the eastern and western parts by the Liupan Mountains. The sections investigated here including the Jingbian, Xifeng, Baoji and Weinan sections, which are in the northern, central, and southern parts of the eastern CLP, respectively (Fig. 1b). For a spatial comparison, we also collated previously reported data from the Dingbian and Luochuan sections in the eastern CLP, and from other five sections in the western CLP: the Gulang, Menyuan, Jingyuan, Lanzhou and Linxia sections (Fig. 1b). Information on all 11 studied sections is shown in Table 1. As suggested by previous studies (e.g., Xiao et al., 2012; Zhang et al., 2021; Zhou et al., 2022), these sections from the CLP are mostly supplied by dust materials from distant (>100 km) source areas, thus reflecting regional atmospheric circulations and climate changes. We did not select the high-sedimentation-rate Mangshan loess section on the North China Plain (Sun et al., 2021) because it is primarily fed by the proximal materials from the lower Yellow River floodplain (Marković et al., 2018; Shang et al., 2018). Considering the significant differences in climate and sedimentation rates, as well as dust provenance, among these 11 sections, these locations are ideal for exploring the impact of provenance differences on recorded climate cycles.

The Jingbian section is located at Guojialiang Village, Jingbian County, Yulin City, Shaanxi Province, in the transition zone between the Mu Us Desert and the northern part of the CLP (Fig. 1). Ding et al. (2005) reported grain size and magnetic susceptibility data from the Jingbian section spanning the past 3.5 Ma. Our section is ~26 km to the south of the section reported by Ding et al. (2005). In this study, we collected samples from the top 88 m (S0–L7 layers) of this section with a sampling interval of 5 cm. During our field investigation, two sedimentary hiatuses were observed in the upper part of L1 (last glacial loess) and the lower part of L2 (penultimate glacial loess), which are likely consistent with the timing of two wind erosion hiatuses determined from high-resolution optically stimulated luminescence dating (Stevens et al., 2018).

The Xifeng section is located in Xifeng District, Qingyang City, Gansu Province, in the central part of the CLP (Fig. 1). The Quaternary loess in this section is about 170 m in thickness. Previous work on this section has investigated magnetostratigraphy, grain size, magnetic susceptibility, free iron/total iron ratio, and ^{10}Be based precipitation estimates (Guo et al., 2000, 2005; Zhou et al., 2023). Here, we collected samples from the top 65.5 m (S0–L7) of the section using a 2–5 cm sampling interval for grain size and magnetic susceptibility analysis.

The Baoji section is located at Linghui Village, Jintai District, Baoji City, Shaanxi Province, in the southern part of the CLP (Fig. 1). The thickness of Quaternary loess in this section is ~160 m. Grain size and magnetic susceptibility data (with 10 cm sampling resolution) from this section have been reported in previous studies (Ding et al., 1994; Meng et al., 2018). Here, we sampled the upper 54 m (S0–L7) of this section with a resolution of 5 cm.

The Weinan section is located at Yanyu Village, Weinan City, Shaanxi Province, in the southern part of the CLP (Fig. 1). The thickness of Quaternary loess in this section is about 170 m, with no sedimentary hiatuses observed (Zhu et al., 2000). Previous studies have reported the results of magnetic susceptibility, magnetostratigraphy, and grain size in this section (Pan et al., 2002; Zhu et al., 2000), as well as biomarker results from the S0-L3 units (Tang et al., 2017). In this study, we measured grain size and magnetic susceptibility on samples from the S0–L7 layers in this section, with a sampling interval of 5 cm.

2.2. Methods

Magnetic susceptibility and grain size are widely used as climate indicators for the summer and winter monsoon, respectively, as well as stratigraphic correlation tools for Chinese loess investigations (An et al., 1990; Ding et al., 1994; Hao et al., 2012; Liu and Ding, 1998; Xiao et al., 1995). In this study, we conducted magnetic susceptibility and grain size analysis on 4742 and 5291 samples, respectively. Low-frequency magnetic susceptibility was measured using a Bartington MS2 magnetometer. The grain size was measured using a Beckman Coulter LS13320 particle size analyzer, which has a measurement range of 0.02–2000 μm with a relative error of <1 % based on repeated measurements. The pretreatment procedure for grain size analysis followed Lu et al. (2002). The magnetic susceptibility and grain size experiments were both carried out in the Soil Geology and Environmental Laboratory of the Institute of Geology and Geophysics, Chinese Academy of Sciences. Spectral analysis of the resultant data was conducted using Acycle software (Li et al., 2019).

Table 1
Details of the loess sections referred in this study.

Loess section	Latitude	Longitude	Stratigraphy and thickness (m)	Accumulation rates (cm/ka)	Mean annual temperature (°C)	Mean annual precipitation (mm)	References
Eastern Chinese Loess Plateau							
Jingbian	37.68°N	108.52°E	S0–L7, 87.3 m	11.80	9.9	450	This study
Dingbian	37.14°N	107.39°E	S0–L5, 117.2 m	26.28	9.3	346	Sun et al., 2021
Xifeng	35.75°N	107.82°E	S0–L7, 65.55 m	8.79	9.9	550	This study
Luochuan	35.75°N	109.42°E	S0–L7, 49 m	6.53	10.3	596	Hao et al., 2012
Baoji	34.25°N	107.07°E	S0–L7, 55.6 m	7.41	12.9	650	This study
Weinan	34.35°N	109.52°E	S0–L7, 50.8 m	6.77	14.0	650	This study
Western Chinese Loess Plateau							
Menyuan	37.33°N	101.82°E	S0–S4, 80.9 m	18.83	0.8	520	Tian et al., 2022
Gulang	37.49°N	102.88°E	S0–S6, 180 m	25.56	5.9	360	Sun et al., 2021
Jingyuan	36.35°N	104.60°E	S0–S6, 180 m	25.78	8.9	240	Sun et al., 2019
Lanzhou	36.10°N	103.44°E	S0–L3, 79.95 m	30.75	10.9	300	Guo et al., 2022
Linxia	35.15°N	103.63°E	S0–L6, 180 m	27.11	9.9	280	Sun et al., 2021

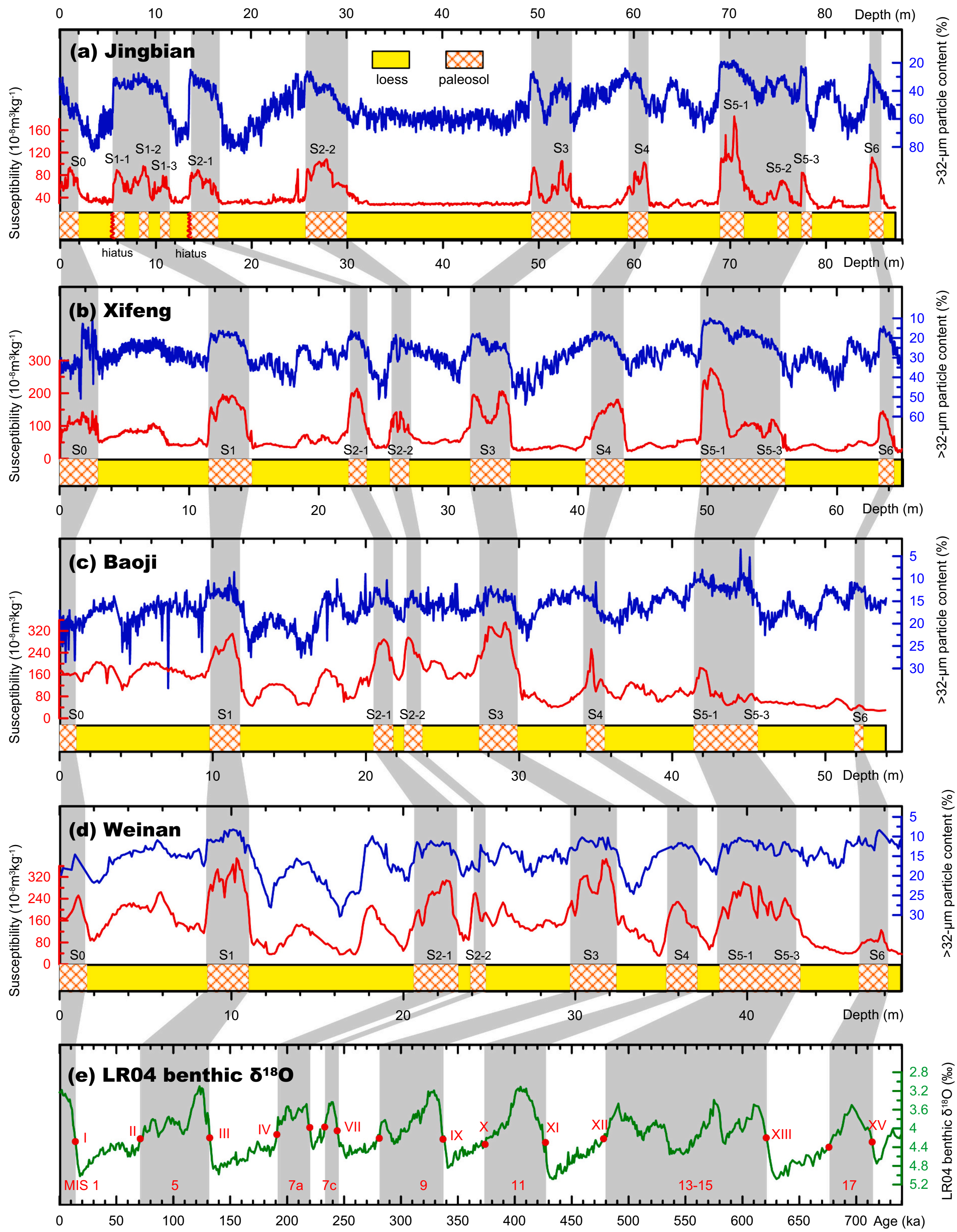

Fig. 2. Comparison of grain size and magnetic susceptibility in the studied sections with the composite marine oxygen isotope curve of Lisiecki and Raymo (2005). The red dots show the age tie points used for correlation. (For interpretation of the references to colour in this figure legend, the reader is referred to the web version of this article.)

3. Results and discussion

3.1. Grain size, magnetic susceptibility, and chronologies of the study sections

Grain size and magnetic susceptibility results for the four sections investigated in this study are shown in Figs. 2a–d. Grain size and magnetic susceptibility of these sections reflect the paleosol and loess units identified in the field, with higher values of magnetic susceptibility and the lower values of grain size in the S0–S6 paleosol units. In general, the magnetic susceptibility and grain size curves of the sections can be readily correlated (Fig. 2). Moreover, magnetic susceptibility is lower overall in sections to the north of the CLP relative to sections in the south, and grain size is higher overall in the north relative to the south,

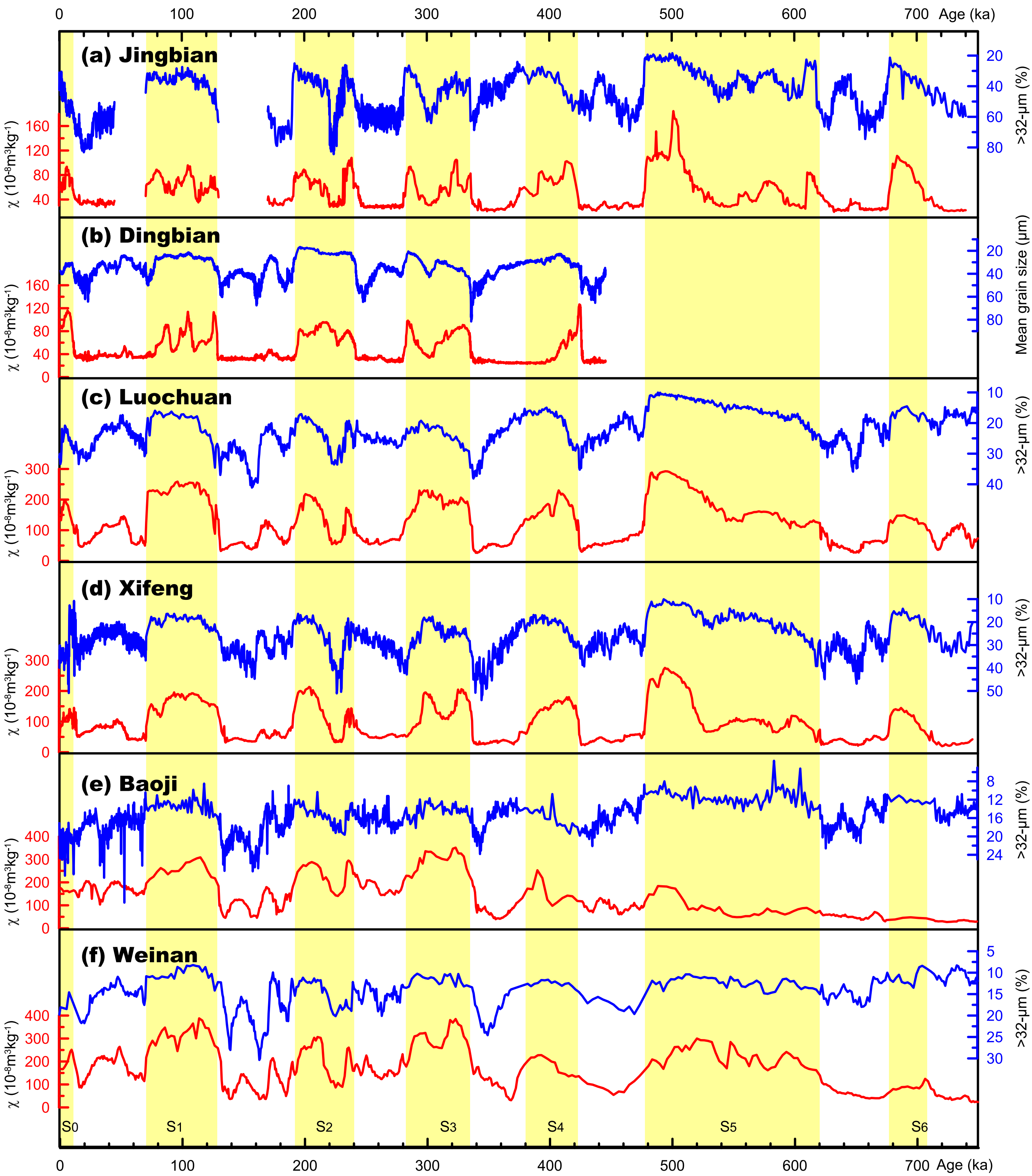

Fig. 3. Comparison of grain size and magnetic susceptibility of different loess sections on the eastern CLP. (a) Jingbian; (b) Dingbian (Sun et al., 2021); (c) Luochuan (Hao et al., 2012); (d) Xifeng; (e) Baoji; and (f) Weinan.

aligning with previous studies (Ding et al., 1995, 2005; Guo et al., 2000; Hao et al., 2012; Meng et al., 2018).

In their pioneering work, Heller and Liu (1984) established a loess chronology spanning the last 0.8 Ma by correlating magnetic susceptibility data with the marine oxygen isotopic record, anchored magnetostratigraphically using the Brunhes-Matuyama boundary. Subsequently, Kukla et al. (1988) correlated the transition boundaries of loess and paleosols with those of marine oxygen isotope stages and established a more accurate chronological framework for the Chinese loess by matching units S0, S1, S2, S3, S4, S5, S6, S7, and S8 to marine oxygen isotope stages MIS1, MIS5, MIS7, MIS9, MIS11, MIS13–15, MIS17, MIS19, and MIS21, respectively. This chronological framework has been consistently confirmed by subsequent studies (Ding et al., 1995, 2002; Hao et al., 2012; Heslop et al., 2000; Pan et al., 2021; Zhang et al.,

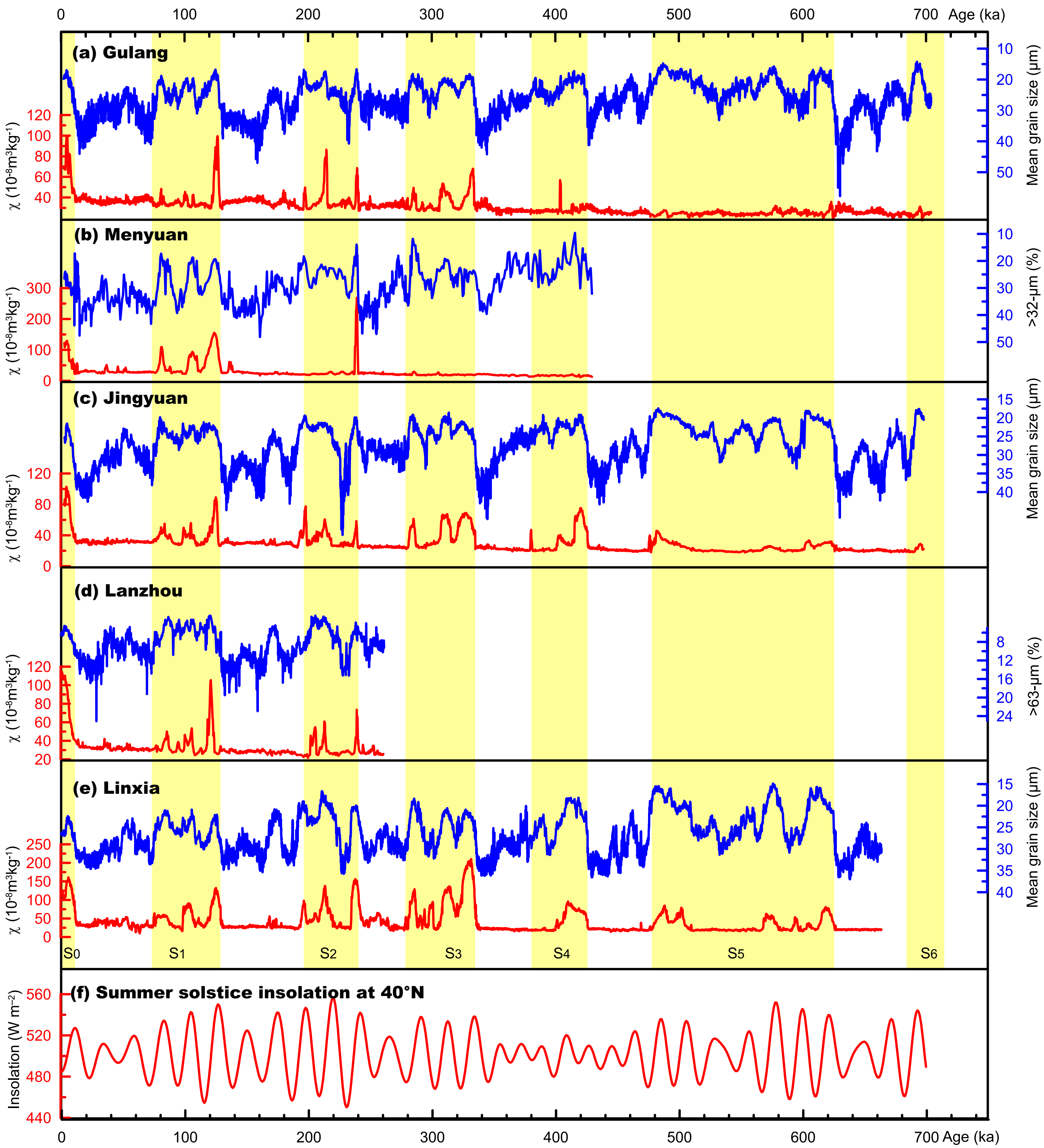

Fig. 4. Grain size and magnetic susceptibility records of different loess sections on the western CLP and comparison with summer solstice insolation at 40°N. (a) Gulang (Sun et al., 2021); (b) Menyuan (Tian et al., 2022; Xiao et al., 2023); (c) Jingyuan (Sun et al., 2021); (d) Lanzhou (Guo et al., 2022); (e) Linxia (Sun et al., 2021); and (f) Summer solstice insolation at 40°N (Berger and Loutre, 1991).

2022b; Zhou and Shackleton, 1999; Zhou et al., 2014). To establish the chronologies of our studied loess sections, we correlate magnetic susceptibility and grain size of our sections with the composite oxygen isotope curve of Lisiecki and Raymo (2005) (LR04), following the chronological framework of recent publications (e.g., Hao et al., 2012; Zhou et al., 2014). Based on detailed correlation, 15 tie points (I–XV) were adopted to refine the chronology of the four sections (Fig. 2e). Our results correspond well to the speleothem oxygen isotope-based chronology for other loess sections (Sun et al., 2021).

3.2. Grain size periodicities of the different loess sections

To explore the periodic variations in grain size and magnetic susceptibility data in different loess sections on the CLP, we further compare the results of our four sections to seven other loess sections with high-precision chronologies, as detailed in Table 1.

Among the six sections on the eastern side of the CLP, the Dingbian and Jingbian sections are in the northern part, the Luochuan and Xifeng sections are in the central part, and the Baoji and Weinan sections are in the southeastern part (see Fig. 1b for locations). As shown in Fig. 3, grain size and magnetic susceptibility of the six sections are generally

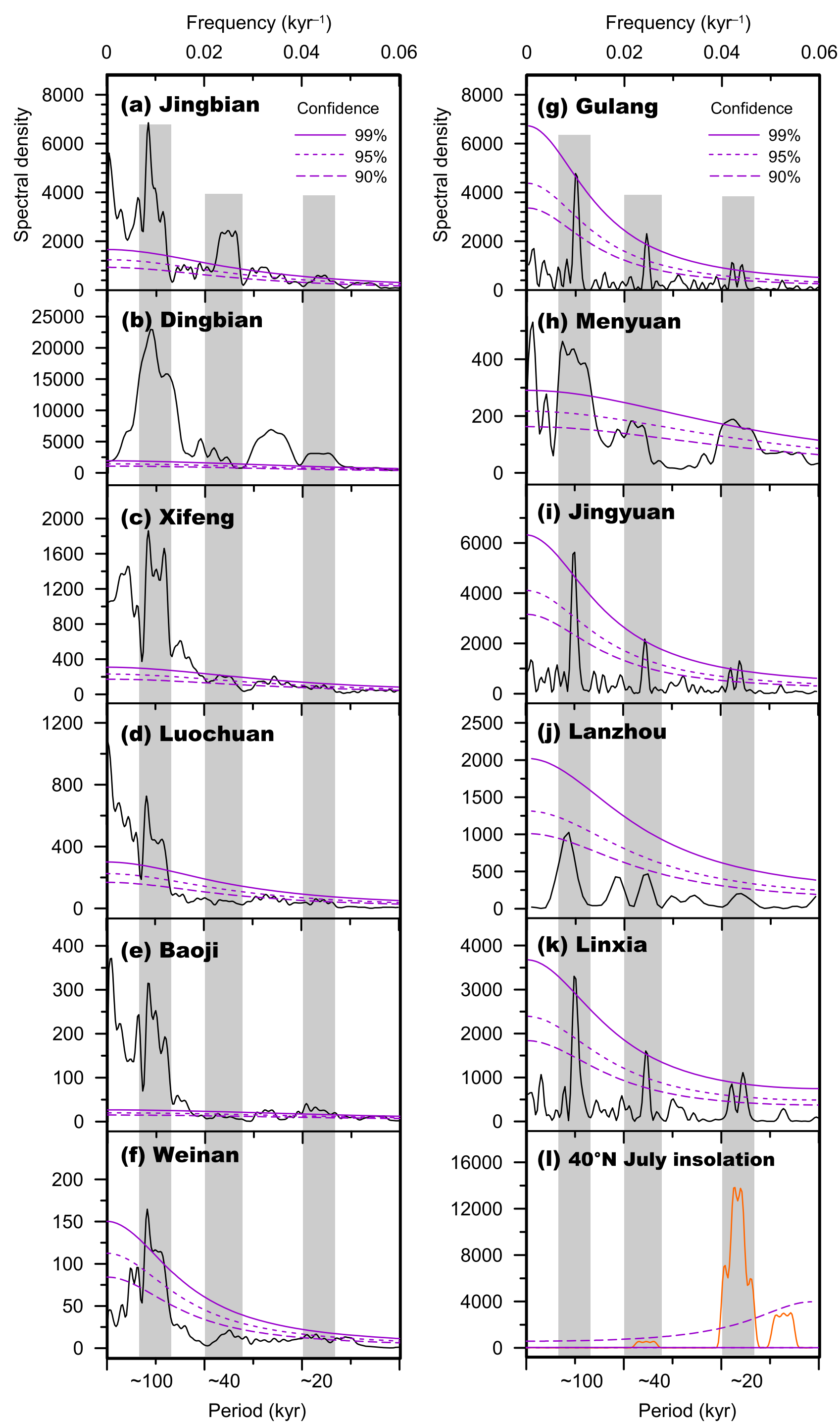

Fig. 5. Comparison of grain size periodicities from different loess sections on the eastern CLP (a–f in the left panel) with those on the western CLP (g–k in the right panel). Note that the ~20-kyr period is more readily apparent in the sections from the western CLP.

comparable, but there are also some differences. For instance, the magnetic susceptibility curves of S1 in the Jingbian and Dingbian sections exhibit three peaks (Figs. 3a, b), which correspond well to three precession cycles, but only one peak exists in the Xifeng, Luochuan, Baoji and Weinan sections (Figs. 3c–f). Similarly, magnetic susceptibility and grain size curves of S3 in the Jingbian and Dingbian sections possess two obvious peaks (Figs. 3a, b), but only one or two peaks in magnetic susceptibility and one peak in grain size in four other sections (Figs. 3c–f). Three magnetic susceptibility peaks and four grain size peaks from the Jingbian section correspond to three paleosol layers of S5, while in other sections, magnetic susceptibility and grain size curves are lack of discernible changes. Ma et al. (2017) attributed this phenomenon to impacts of sedimentation rate and pedogenesis. In the sections with low sedimentation rate and relatively strong pedogenesis, multiple sub-soil layers in the same stratigraphic unit can be merged into a single soil layer, leading to one peak in magnetic susceptibility curve; whereas in the northern CLP, these sub-soil layers do not merge into a soil layer due to high sedimentation rate and weaker pedogenesis, and thus the magnetic susceptibility curve displays multiple peaks.

The sedimentation rate is high in the 5 loess sections from the western CLP, with 4 of them exceeding 25 cm/ka (Table 1). The values of magnetic susceptibility in these sections are generally lower compared to the 6 sections on the eastern CLP, and some paleosol units (e.g., S4 and S5) exhibit less prominent magnetic susceptibility peaks (Fig. 4), which could be attributed to reduced precipitation and weaker pedogenesis in these regions. In these sections, multiple sub-paleosols did not merge with each other to became a composite soil unit. It is noteworthy that grain size variations of these sections are distinct from those observed in the 6 loess sections on the eastern CLP. For example, magnetic susceptibility and grain size of S1 and S3 units both exhibit three peaks in these sections, which correspond well with three coeval precession cycles in insolation (Fig. 4). However, the grain size of all six sections on the eastern CLP do not show these precession cycles (Fig. 3). Although there is an absence of discernible changes in magnetic susceptibility, the grain size records of S5 units on the western CLP exhibit significant variations, which may be related to precession cycles (Fig. 4). In contrast, there are no significant changes in grain size records of the six sections on the eastern CLP (Fig. 3).

Spectral analysis of grain size records from the six sections on the eastern CLP reveals a dominant ~100-kyr ice-age cycle and relatively damped ~20-kyr precession cycles (Figs. 5a–f). In contrast, ~100-kyr and ~ 20-kyr cycles are both significant in grain size records from the western CLP (Figs. 5g–k), demonstrating that there are differences in grain size periodicity between the eastern and western CLP, with precession cycles more obvious in the western CLP. This discrepancy is probably due to the presence of distinct precession cycles in the grain size records of the same soil unit (e.g., S1, S3, and S5) within sections from the western CLP, whereas these soil units from the eastern CLP lack precession cycle variability. Importantly, this difference cannot be simply explained by the low sedimentation rate and strong pedogenesis of the eastern CLP, because the Dingbian and Jingbian sections in the northern part of the eastern CLP have high sedimentation rates and weak pedogenesis (Table 1), yet still lack precession cycles in grain size records, although the magnetic susceptibility of S1 and S3 units display precession cycles. Additionally, all 11 sections across the CLP display a relatively damped ~40-kyr cycle in the grain-size records (Figs. 5a–k), which is undoubtedly corresponds to the 41-kyr obliquity cycle (Berger and Loutre, 1991).

3.3. Climate significance of periodic variations in loess grain size

The above results reveal that the grain size variations both from the eastern and western CLP show a dominant ~100-kyr ice-age cycle. However, the precession signal on the western CLP is more obvious compared to the eastern part of the CLP. We propose that the precession signals in loess sections on the western CLP were not related to the summer monsoon. This hypothesis is supported by several lines of evidence: 1) loess particles are mainly transported by the winter monsoon or Westerlies, and grain size cannot be employed as an indicator of summer monsoon (Xiao et al., 1995; Hao et al., 2012), and 2) summer monsoon precipitation exerts a more pronounced impact on the eastern CLP, while exerting a comparatively weaker impact on the western CLP (Ma et al., 2017).

Previous studies suggest that the grain size variations across the CLP were controlled by the strength of the wind and the distance from the source area (Ding et al., 1999, 2005). The dominant ~100-kyr cycle in the grain size records of the eastern and western CLP was derived from the variations of Northern Hemisphere ice volume, which can transmit the ~100-kyr ice-age signal to the CLP and other regions in East Asia by regulating the changes in the intensity of the Siberia-Mongolia high-pressure and winter monsoon (Ding et al., 1995; Hao et al., 2012), as shown in Fig. 6. However, because ~20-kyr precession cycles are only clear in grain size records on the western CLP, it suggests that this climate signal may not be related to the winter monsoon and variations of Northern Hemisphere ice volume/Siberia-Mongolia high-pressure. Rather the signal is probably related to some other, more localized process(es).

One important clue is that the paleoclimate changes over the western CLP are influenced not only by the Siberia-Mongolia high-pressure system, but also by the Tibetan Plateau and Westerlies (Fig. 6), because this region is close to the Tibetan Plateau and central Asia. A growing body of climate simulations and geological evidence suggest that climate changes in Westerlies-dominated region and Tibetan Plateau show dominant ~100-kyr ice-age cycles and significant ~20-kyr precession cycles (Fig. 7). For example, modeling reconstructions (Fig. 7a) for central Asia shown significant precession cycles in temperature and precipitation (Li et al., 2013; Liu et al., 2022), which correspond well to periodic variations in precipitation inferred by speleothem data (Fig. 7b) in the region (Cheng et al., 2012, 2016). Moreover, various proxies from Lake Ohrid in the Mediterranean region (Fig. 7c) indicate that, in addition to ~100-kyr ice-age cycle, ~20-kyr precession cycles were also recorded in this region over the last 0.7 Ma (Wagner et al., 2019). The ~100-kyr ice-age and ~ 20-kyr precession cycles were also documented in high-resolution pollen data from the Zoige Basin on the Tibetan Plateau (Fig. 7d) (Zhao et al., 2020). Therefore, the precession signals in loess grain size in the western CLP are most probably derived from the Westerlies-dominated region and Tibetan Plateau.

Recent investigations reveal that the deserts located on the Northeastern Tibetan Plateau (e.g., Qaidam Basin, Tengger, and Badain Jaran) and to the north of the CLP (e.g., Mu Us Desert and Gobi in Southern Mongolia) were important source areas for the loess on the CLP (Che and Li, 2013; Maher et al., 2009; Pullen et al., 2011; Sun et al., 2008, 2020; Xiao et al., 2012; Zhang et al., 2021, 2022a; Zhou et al., 2022). However, under the influence of East Asian winter monsoon and Westerlies, source areas for the loess on the western CLP were different from those on the eastern CLP (Fig. 6). There was relatively more dust on the western CLP derived from the Northeastern Tibetan Plateau region; By contrast, dust on the eastern CLP mostly came from the deserts in northern China and Gobi in southern Mongolia (Xiao et al., 2012; Zhang et al., 2021; Zhou et al., 2022). As noted above, the climate variations in the Westerlies-dominated region and Tibetan Plateau are influenced by the ~100-kyr ice-age cycle as well as ~20-kyr precession cycles, and thus it makes sense that the dust from these regions exhibits these cycles. These periodic signals could be transmitted and recorded in the loess grain size records of the western CLP via variations in the size of the source areas, strength of wind, dust flux. Recently, Xiao et al. (2023) compared the grain size and provenance of the Luochuan loess to those of Menyuan loess in the eastern part of the Qilian Mountains, and suggested that Menyuan loess was mainly derived from the Northeastern Tibetan Plateau, and dust supply was related to alpine glaciation activities in the Northeastern Tibetan Plateau that were driven by local summer insolation. Therefore, the grain size record of Menyuan loess displays

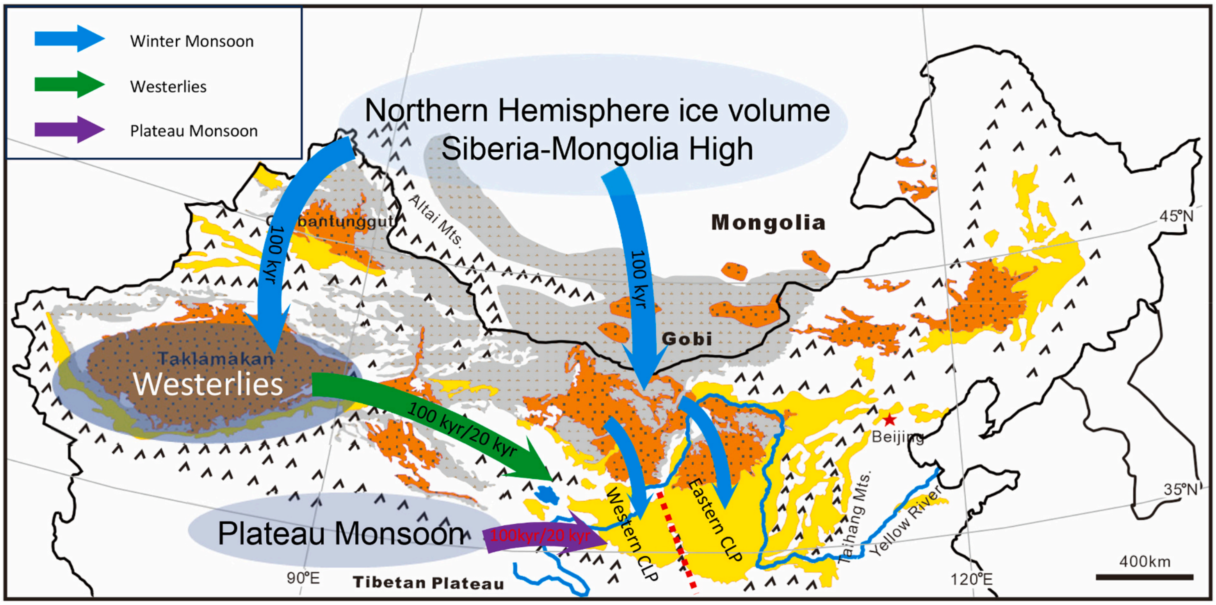

Fig. 6. A conceptual model for the mechanism that can explain different loess grain-size periodicities preserved on the eastern versus western CLP. The legends are same as Fig. 1b.

significant ~20-kyr precession cycles, which is obviously different from the predominant ~100-kyr ice-age cycles of the Luochuan loess on the eastern CLP.

The dust source for loess on the eastern CLP was mainly derived from the Mu Us Deserts and Gobi in Southern Mongolia, with less dust sourced from the Northeastern Tibetan Plateau (Xiao et al., 2012; Zhang et al., 2021; Zhou et al., 2022), and dust transportation was mainly controlled by the East Asian winter monsoon, which is regulated by Siberia-Mongolia high-pressure that is itself strongly modulated by ~100-kyr ice-age cycles (Ding et al., 1995; Hao et al., 2012). This can explain why grain-size records from the eastern CLP show dominant ~100-kyr ice-age cycles, but lack ~20-kyr precession cycles. For the damped ~40-kyr obliquity cycles in the grain-size records of both eastern and western CLP, these cycles are likely derived from their respective source regions. Geological records from Northern Hemisphere high latitudes (e.g., Williams et al., 1997), central Asia (Fig. 7a), and Tibetan Plateau (Fig. 7d) show clear obliquity cycles. These periodic signals from these regions could be transmitted and recorded in the loess grain-size records of the CLP.

A growing body of evidence supports our view that periodic variations of dust accumulation are influenced by climate changes in dust source areas. For example, the climate record from the MD03–2705 core in the east coast of the Atlantic reveals that dust changes in the Sahara Desert show pronounced ~20-kyr cycles, but lack ~100-kyr cycles (Skonieczny et al., 2019), which is in-line with the climate variations recorded in the low-latitude region of Africa (Kutzbach et al., 2008). In contrast to the Sahara Desert, the climate during the last 0.8 Ma in South America was dominated by ~100-kyr age-age cycles (Rodbell et al., 2022), and the deserts in the South America are the main source regions for dusts in equatorial eastern Pacific and Southern Ocean, south Atlantic, and Antarctic regions (Delmonte et al., 2008; Delmonte et al., 2004; Lamy et al., 2014). Dust concentration variations from the ODP 1090 core in south Atlantic (Martínez-Garcia et al., 2011), ODP 849 core in equatorial eastern Pacific (Winckler et al., 2008), and Dome C ice core in Antarctica (Lambert et al., 2008), all display a dominant ~100-kyr cycle during the last 0.8 Ma, but lack ~20-kyr cycles, in agreement with the climate variations recorded in South America.

3.4. Implications for regional paleoclimatic reconstruction

Our findings provide at least two valuable implications for regional paleoclimate reconstruction based on investigations of CLP loess-paleosol sequences. Firstly, loess grain size is a widely accepted proxy of the East Asian winter monsoon (Ding et al., 1994; Hao et al., 2012; Liu and Ding, 1998; Xiao et al., 1995) yet our study indicates that grain size variability in loess cannot be simply explained by changes in the East Asian winter monsoon. As such, the climatic significance of loess grain size on the CLP should be specified according to its location. Secondly, previous studies on Asian paleoclimate changes often use only one loess section on the CLP to represent the whole mid-latitude monsoon region, and these studies tend to overlook the climate differences among different parts of the CLP, as demonstrated in this study. Recent studies demonstrate that the dominant orbital periodicities of the East Asian summer monsoon during the late Quaternary, as recorded by loess on the CLP and at lower latitudes were different (Bao et al., 2022; Guo et al., 2000; Li et al., 2024), further indicating how the characteristics and forcing factors of Asian climate are spatially diverse.

4. Conclusions

Our comparison of six loess sections in the eastern Chinese Loess Plateau (CLP) to five loess sections in the western CLP spanning the past 0.7 Ma reveals key differences in the preserved orbital signals. We found that the dominant periodicity in grain size data on the eastern CLP is the ~100-kyr ice-age cycle, with only a very weak precession signal preserved, whilst the western CLP exhibits both ~100-kyr ice-age cycles and significant ~20 kyr precession cycles. This spatial difference in periodicity cannot be attributed to any differences in accumulation rates and/or the merging of sub-soil layers caused by pedogenesis. We propose instead that the differences in the orbital responses in different parts of the CLP can be attributed to the differences in the climatic signals from the respective dust source areas, which regulated particle sizes. The loess on the eastern CLP is derived largely from deserts to the north (e.g., Mu Us Desert and Gobi Desert in south Mongolia), with climates that are controlled by the Siberia-Mongolia high-pressure that was modulated by ~100-kyr cycle, without significant influence from ~20-kyr precession. By contrast, the loess on the western CLP is mainly derived from the Northeastern Tibetan Plateau, and the production,

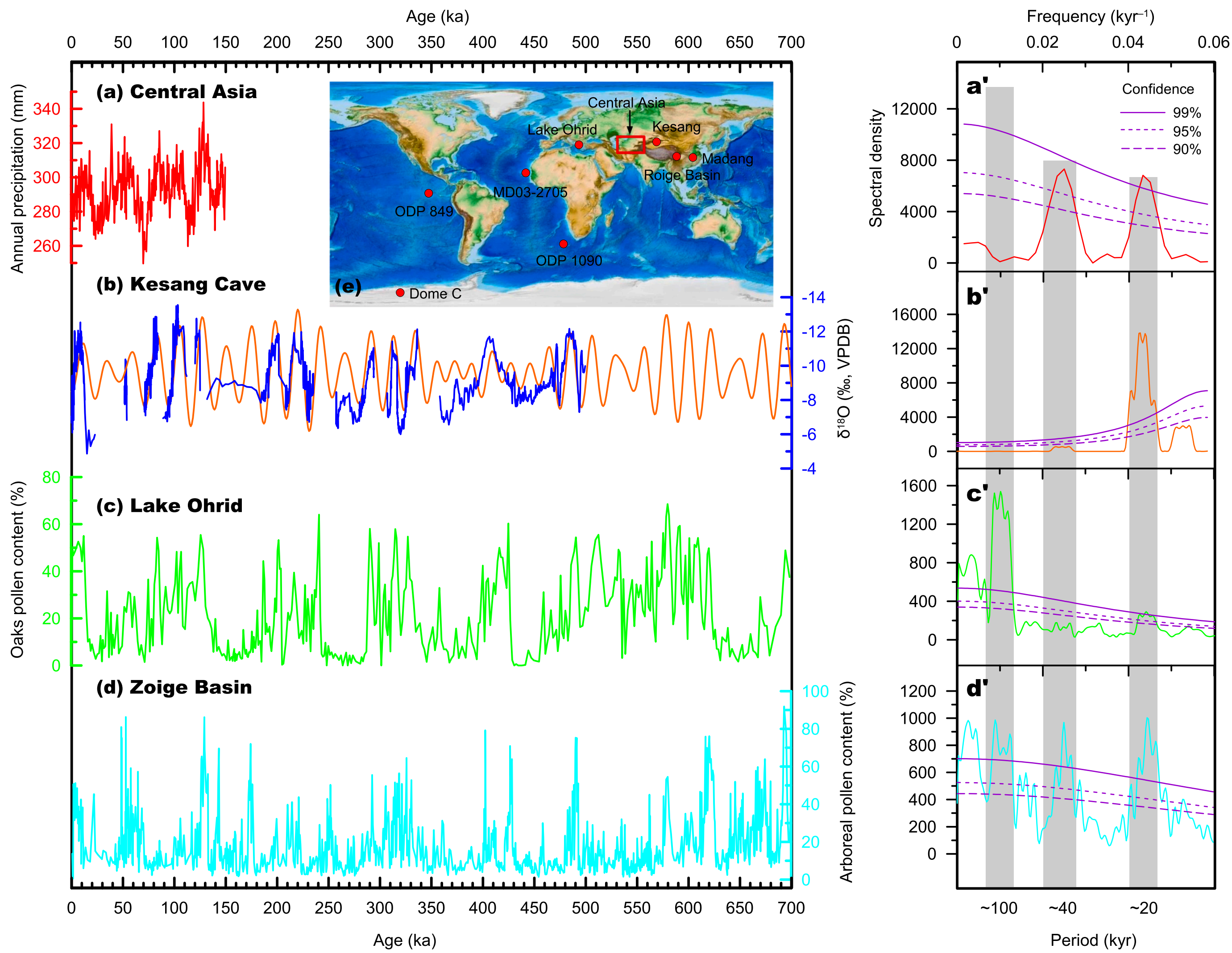

Fig. 7. Climate variations and their periodic characteristics in Westerlies-dominated region and Tibetan Plateau. (a) Central Asia annual precipitation from the simulation (Li et al., 2013); (b) The speleothem $\delta^{18}O$ record from the Kesang Cave (Cheng et al., 2012), and the orange curve is the summer solstice insolation at 40°N (Berger and Loutre, 1991); (c) Percentage of pollen from deciduous oaks at Lake Ohrid (Wagner et al., 2019); and (d) Arboreal pollen percentages from the Zoige Basin, Tibetan Plateau (Zhao et al., 2020). The right panels show the power spectral analyses for the palaeoclimatic records in the left panels. The inset map in the left panel shown the locations of these records.

transportation, and accumulation of the dusts there are influenced by both ~100-kyr ice-age cycles and ~ 20-kyr precession. Our study highlights how the climate variability encoded in Chinese loess was spatially diverse, and strongly influenced by the climate variability of the source regions.

CRediT authorship contribution statement

Deai Zhao: Writing – review & editing, Writing – original draft, Investigation, Formal analysis, Data curation. **Guoqiao Xiao:** Writing – review & editing, Investigation, Funding acquisition, Formal analysis, Conceptualization. **Chunju Huang:** Writing – review & editing, Funding acquisition, Formal analysis. **Haibin Wu:** Writing – review & editing, Resources. **Qingzhen Hao:** Resources, Methodology. **David B. Kemp:** Writing – review & editing. **Shaohua Tian:** Validation, Investigation. **Zhipeng Wu:** Validation, Investigation. **Hao Lu:** Investigation. **Gaowen Dai:** Investigation. **Shuzhen Peng:** Methodology. **Changyan Tang:** Investigation. **Jianyu Wu:** Investigation. **Yating Lin:** Investigation. **Shuya Zhu:** Investigation. **Qiuzhen Yin:** Methodology.

Declaration of competing interest

The authors declare that they have no known competing financial interests or personal relationships that could have appeared to influence the work reported in this paper.

Data availability

Data will be made available on request.

Acknowledgments

This study is supported by the National Natural Science Foundation of China (Grant nos. 42488201, 42272217, 42230208) and the Fonds de la Recherche Scientifique FNRS (F.R.S.-FNRS) under grant MIS F.4529.18. Z. Wu is supported by the F.R.S.-FNRS grant no. T.0246.23. Q. Yin is Senior Research Associate of F.R.S.-FNRS.

References

An, Z.S., Liu, T.S., Lu, Y.C., Porter, S.C., Kukla, G., Wu, X.H., Hua, Y.M., 1990. The long-term paleomonsoon variation recorded by the loess-paleosol sequence in Central China. Quat. Int. 7–8, 91–95. https://doi.org/10.1016/1040-6182(90)90042-3.

Bao, R., Sheng, X., Meng, X., Li, T., Li, C., Shen, H., Da, J., Ji, J., Chen, J., 2022. 100 k.y. pacing of the East Asian summer monsoon over the past five glacial cycles inferred from land snails. Geology 51, 179–183. https://doi.org/10.1130/G50243.1.

Beck, J.W., Zhou, W., Li, C., Wu, Z., White, L., Xian, F., Kong, X., An, Z., 2018. A 550,000-year record of East Asian monsoon rainfall from ^{10}Be in loess. Science 360, 877–881. https://doi.org/10.1126/science.aam5825.

Berger, A., Loutre, M.F., 1991. Insolation values for the climate of the last 10 million years. Quat. Sci. Rev. 10, 297–317. https://doi.org/10.1016/0277-3791(91)90033-Q.

Che, X., Li, G., 2013. Binary sources of loess on the Chinese Loess Plateau revealed by U–Pb ages of zircon. Quat. Res. 80, 545–551. https://doi.org/10.1016/j.yqres.2013.05.007.

Cheng, H., Zhang, P.Z., Spötl, C., Edwards, R.L., Cai, Y.J., Zhang, D.Z., Sang, W.C., Tan, M., An, Z.S., 2012. The climatic cyclicity in semiarid-arid Central Asia over the past 500,000 years. Geophys. Res. Lett. 39, L01705. https://doi.org/10.1029/2011GL050202.

Cheng, H., Spotl, C., Breitenbach, S.F., Sinha, A., Wassenburg, J.A., Jochum, K.P., Scholz, D., Li, X., Yi, L., Peng, Y., Lv, Y., Zhang, P., Votintseva, A., Loginov, V., Ning, Y., Kathayat, G., Edwards, R.L., 2016. Climate variations of Central Asia on orbital to millennial timescales. Sci. Rep. 5, 36975. https://doi.org/10.1038/srep36975.

Delmonte, B., Basile-Doelsch, I., Petit, J.R., Maggi, V., Revel-Rolland, M., Michard, A., Jagoutz, E., Grousset, F., 2004. Comparing the Epica and Vostok dust records during the last 220,000 years: stratigraphical correlation and provenance in glacial periods. Earth Sci. Rev. 66, 63–87. https://doi.org/10.1016/j.earscirev.2003.10.004.

Delmonte, B., Andersson, P.S., Hansson, M., Schöberg, H., Petit, J.R., Basile-Doelsch, I., Maggi, V., 2008. Aeolian dust in East Antarctica (EPICA-Dome C and Vostok): Provenance during glacial ages over the last 800 kyr. Geophys. Res. Lett. 35, L07703. https://doi.org/10.1029/2008GL033382.

Ding, Z.L., Yu, Z.W., Rutter, N.W., Liu, T.S., 1994. Towards an orbital time scale for Chinese loess deposits. Quat. Sci. Rev. 13, 39–70. https://doi.org/10.1016/0277-3791(94)90124-4.

Ding, Z.L., Liu, T.S., Rutter, N.W., Yu, Z.W., Guo, Z.T., Zhu, R.X., 1995. Ice-volume forcing of east Asian winter monsoon variations in the past 800,000 years. Quat. Res. 44, 149–159. https://doi.org/10.1006/qres.1995.1059.

Ding, Z.L., Sun, J.M., Rutter, N.W., Rokosh, D., Liu, T.S., 1999. Changes in sand content of loess deposits along a north-south transect of the Chinese Loess Plateau and the implications for desert variations. Quat. Res. 52, 56–62. https://doi.org/10.1006/qres.1999.2045.

Ding, Z.L., Derbyshire, E., Yang, S.L., Yu, Z.W., Xiong, S.F., Liu, T.S., 2002. Stacked 2.6-Ma grain size record from the Chinese loess based on five sections and correlation with the deep-sea δ^{18}O record. Paleoceanography 17, 1033. https://doi.org/10.1029/2001PA000725.

Ding, Z.L., Derbyshire, E., Yang, S.L., Sun, J.M., Liu, T.S., 2005. Stepwise expansion of desert environment across northern China in the past 3.5 Ma and implications for monsoon evolution. Earth Planet. Sci. Lett. 237, 45–55. https://doi.org/10.1016/j.epsl.2005.06.036.

Guo, Z.T., Biscaye, P., Wei, L.Y., Chen, X.H., Peng, S.Z., Liu, T.S., 2000. Summer monsoon variations over the last 1.2 Ma from the weathering of loess-soil sequences in China. Geophys. Res. Lett. 27, 1751–1754. https://doi.org/10.1029/1999GL008419.

Guo, Z.T., Ruddiman, W.F., Hao, Q.Z., Wu, H.B., Qiao, Y.S., Zhu, R.X., Peng, S.Z., Wei, J.J., Yuan, B.Y., Liu, T.S., 2002. Onset of Asian desertification by 22 Myr ago inferred from loess deposits in China. Nature 416, 159–163. https://doi.org/10.1038/416159a.

Guo, Z.T., Hao, Q.Z., Wei, J.J., An, Z.S., 2005. Astronomical signals in different climate proxies from the Quaternary loess-soil sequences in China. In: Berger, A., Ercegovac, M., Mesinger, F. (Eds.), Proceedings of the Milutin Milankovitch anniversary Symposium: Paleoclimate and the Earth Climate System, pp. 101–111. Belgrade.

Guo, B., Nie, J., Stevens, T., Buylaert, J.-P., Peng, T., Xiao, W., Pan, B., Fang, X., 2022. Dominant precessional forcing of the East Asian summer monsoon since 260 ka. Geology 50, 1372–1376. https://doi.org/10.1130/G50206.1.

Hao, Q., Wang, L., Oldfield, F., Peng, S., Qin, L., Song, Y., Xu, B., Qiao, Y., Bloemendal, J., Guo, Z., 2012. Delayed build-up of Arctic ice sheets during 400,000-year minima in insolation variability. Nature 490, 393–396. https://doi.org/10.1038/nature11493.

Heller, F., Liu, T.S., 1984. Magnetism of Chinese loess deposits. Geophys. J. R. Astron. Soc. 77, 125–141. https://doi.org/10.1111/j.1365-246X.1984.tb01928.x.

Heslop, D., Langereis, C.G., Dekkers, M.J., 2000. A new astronomical timescale for the loess deposits of Northern China. Earth Planet. Sci. Lett. 184, 125–139. https://doi.org/10.1016/S0012-821X(00)00324-1.

Kukla, G., Heller, F., Liu, X.M., Xu, T.C., Liu, T.S., An, Z.S., 1988. Pleistocene climates in China dated by magnetic susceptibility. Geology 16, 811–814. https://doi.org/10.1130/0091-7613(1988)016<0811:PCICDB>2.3.CO;2.

Kutzbach, J.E., Liu, X.D., Liu, Z.Y., Chen, G.S., 2008. Simulation of the evolutionary response of global summer monsoons to orbital forcing over the past 280,000 years. Clim. Dyn. 30, 567–579. https://doi.org/10.1007/s00382-007-0308-z.

Lambert, F., Delmonte, B., Petit, J.R., Bigler, M., Kaufmann, P.R., Hutterli, M.A., Stocker, T.F., Ruth, U., Steffensen, J.P., Maggi, V., 2008. Dust-climate couplings over the past 800,000 years from the EPICA Dome C ice core. Nature 452, 616–619. https://doi.org/10.1038/nature06763.

Lamy, F., Gersonde, R., Winckler, G., Esper, O., Jaeschke, A., Kuhn, G., Ullermann, J., Martinez-Garcia, A., Lambert, F., Kilian, R., 2014. Increased dust deposition in the Pacific Southern Ocean during glacial periods. Science 343, 403–407. https://doi.org/10.1126/science.1245424.

Li, X., Liu, X., Qiu, L., An, Z., Yin, Z.Y., 2013. Transient simulation of orbital-scale precipitation variation in monsoonal East Asia and arid Central Asia during the last 150 ka. J. Geophys. Res. Atmos. 118, 7481–7488. https://doi.org/10.1002/jgrd.50611.

Li, M., Hinnov, L., Kump, L., 2019. Acycle: Time-series analysis software for paleoclimate research and education. Comput. Geosci. 127, 12–22. https://doi.org/10.1016/j.cageo.2019.02.011.

Li, X., Zhou, Y., Han, Z., Yuan, X., Yi, S., Zeng, Y., Qin, L., Lu, M., Lu, H., 2024. Loess deposits in the low latitudes of East Asia reveal the ~20-kyr precipitation cycle. Nat. Commun. 15, 1023. https://doi.org/10.1038/s41467-024-45379-9.

Lisiecki, L.E., Raymo, M.E., 2005. A Pliocene-Pleistocene stack of 57 globally distributed benthic d^{18}O records. Paleoceanography 20, PA1003. https://doi.org/10.1029/2004PA001071.

Liu, T.S., 1985. Loess and the Environment. China Ocean Press, Beijing, p. 251.

Liu, T.S., Ding, Z.L., 1998. Chinese loess and the paleomonsoon. Annu. Rev. Earth Planet. Sci. 26, 111–145. https://doi.org/10.1146/annurev.earth.26.1.111.

Liu, X., Xie, X., Guo, Z., Yin, Z.Y., Chen, G., 2022. Model-based orbital-scale precipitation δ^{18}O variations and distinct mechanisms in Asian monsoon and arid regions. Natl. Sci. Rev. 9, nwac182. https://doi.org/10.1093/nsr/nwac182.

Lu, H.Y., Miao, X.D., Sun, Y.B., 2002. Pretreatment methods and their influences on grain-size measurement of aeolian 'Red Clay' in North China. Mar. Geol. Quat. Geol. 22, 129–135 (in Chinese with English abstract).

Lu, H., Wang, X., Ma, H., Tan, H., Vandenberghe, J., Miao, X., Li, Z., Sun, Y., An, Z., Cao, G., 2004a. The Plateau Monsoon variation during the past 130 kyr revealed by loess deposit at northeast Qinghai–Tibet (China). Glob. Planet. Chang. 41, 207–214. https://doi.org/10.1016/j.gloplacha.2004.01.006.

Lu, H.Y., Zhang, F.Q., Liu, X.D., Duce, R.A., 2004b. Periodicities of palaeoclimatic variations recorded by loess-paleosol sequences in China. Quat. Sci. Rev. 23, 1891–1900. https://doi.org/10.1016/j.quascirev.2004.06.005.

Lu, H., Wang, X., Wang, Y., Zhang, X., Yi, S., Wang, X., Stevens, T., Kurbanov, R., Marković, S.B., 2022. Chinese loess and the Asian monsoon: what we know and what remains unknown. Quat. Int. 620, 85–97. https://doi.org/10.1016/j.quaint.2021.04.027.

Ma, L., Li, Y., Liu, X., Sun, Y., 2017. Registration of precession signal in the last interglacial paleosol (S_1) on the Chinese Loess Plateau. Geochem. Geophys. Geosyst. 18, 3964–3975. https://doi.org/10.1002/2017GC006964.

Maher, B.A., Mutch, T.J., Cunningham, D., 2009. Magnetic and geochemical characteristics of Gobi Desert surface sediments: Implications for provenance of the Chinese Loess Plateau. Geology 37, 279–282. https://doi.org/10.1130/G25293A.1.

Marković, S.B., Stevens, T., Mason, J., Vandenberghe, J., Yang, S., Veres, D., Újvári, G., Timar-Gabor, A., Zeeden, C., Guo, Z., Hao, Q., Obreht, I., Hambach, U., Wu, H., Gavrilov, M.B., Rolf, C., Tomić, N., Lehmkuhl, F., 2018. Loess correlations – between myth and reality. Palaeogeogr. Palaeoclimatol. Palaeoecol. 509, 4–23. https://doi.org/10.1016/j.palaeo.2018.04.018.

Martínez-Garcia, A., Rosell-Melé, A., Jaccard, S.L., Geibert, W., Sigman, D.M., Haug, G.H., 2011. Southern Ocean dust-climate coupling over the past four million years. Nature 476, 312–315. https://doi.org/10.1038/nature10310.

Meng, X., Liu, L., Wang, X.T., Balsam, W., Chen, J., Ji, J., 2018. Mineralogical evidence of reduced East Asian summer monsoon rainfall on the Chinese loess plateau during the early Pleistocene interglacials. Earth Planet. Sci. Lett. 486, 61–69. https://doi.org/10.1016/j.epsl.2017.12.048.

Pan, Y.X., Zhu, R.X., Liu, Q.S., Guo, B., Yue, L.P., Wu, H.N., 2002. Geomagnetic episodes of the last 1.2 Myr recorded in Chinese loess. Geophys. Res. Lett. 29, 1282. https://doi.org/10.1029/2001GL014024.

Pan, Q., Xiao, G., Zhao, Q., Chen, R., Ao, H., Shen, Y., Cheng, J., Zhu, Z., 2021. The Jaramillo subchron in Chinese loess-paleosol sequences. Palaeogeogr. Palaeoclimatol. Palaeoecol. 572, 110423. https://doi.org/10.1016/j.palaeo.2021.110423.

Pullen, A., Kapp, P., McCallister, A.T., Chang, H., Gehrels, G.E., Garzione, C.N., Heermance, R.V., Ding, L., 2011. Qaidam Basin and northern Tibetan Plateau as dust sources for the Chinese Loess Plateau and paleoclimatic implications. Geology 39, 1031–1034. https://doi.org/10.1130/g32296.1.

Rodbell, D.T., Hatfield, R.G., Abbott, M.B., Chen, C.Y., Woods, A., Stoner, J.S., McGee, D., Tapia, P.M., Bush, M., Valero-Garces, B.L., Lehmann, S.B., Mark, S.Z., Weidhaas, N.C., Hillman, A.L., Larsen, D.J., Delgado, G., Katz, S.A., Solada, K.E., Morey, A.E., Finkenbinder, M., Valencia, B., Rozas-Davila, A., Wattrus, N., Colman, S.M., Bustamante, M.G., Kuck, J., Pierdominici, S., 2022. 700,000 years of tropical Andean glaciation. Nature 607, 301–306. https://doi.org/10.1038/s41586-022-04873-0.

Shang, Y., Prins, M.A., Beets, C.J., Kaakinen, A., Lahaye, Y., Dijkstra, N., Rits, D.S., Wang, B., Zheng, H., van Balen, R.T., 2018. Aeolian dust supply from the Yellow River floodplain to the Pleistocene loess deposits of the Mangshan Plateau, Central China: evidence from zircon U-Pb age spectra. Quat. Sci. Rev. 182, 131–143. https://doi.org/10.1016/j.quascirev.2018.01.001.

Skonieczny, C., McGee, D., Winckler, G., Bory, A., Bradtmiller, L.I., Kinsley, C.W., Polissar, P.J., Pol-Holz, R.D., Rossignol, L., Malaizé, B., 2019. Monsoon-driven Saharan dust variability over the past 240,000 years. Sci. Adv. 5, eaav1887. https://doi.org/10.1126/sciadv.aav1887.

Stevens, T., Buylaert, J.P., Thiel, C., Ujvari, G., Yi, S., Murray, A.S., Frechen, M., Lu, H., 2018. Ice-volume-forced erosion of the Chinese Loess Plateau global Quaternary stratotype site. Nat. Commun. 9, 983. https://doi.org/10.1038/s41467-018-03329-2.

Sun, Y.B., Clemens, S.C., An, Z.S., Yu, Z.W., 2006. Astronomical timescale and palaeoclimatic implication of stacked 3.6-Myr monsoon records from the Chinese Loess Plateau. Quat. Sci. Rev. 25, 33–48. https://doi.org/10.1016/j.quascirev.2005.07.005.

Sun, Y.B., Tada, R., Chen, J., Liu, Q.S., Toyoda, S., Tani, A., Ji, J.F., Isozaki, Y., 2008. Tracing the provenance of fine-grained dust deposited on the central Chinese Loess Plateau. Geophys. Res. Lett. 35, L01804. https://doi.org/10.1029/2007GL031672.

Sun, Y., Yin, Q., Crucifix, M., Clemens, S.C., Araya-Melo, P., Liu, W., Qiang, X., Liu, Q., Zhao, H., Liang, L., Chen, H., Li, Y., Zhang, L., Dong, G., Li, M., Zhou, W., Berger, A., An, Z., 2019. Diverse manifestations of the mid-Pleistocene climate transition. Nat. Commun. 10, 352. https://doi.org/10.1038/s41467-018-08257-9.

Sun, Y., Yan, Y., Nie, J., Li, G., Shi, Z., Qiang, X., Chang, H., An, Z., 2020. Source-to-sink fluctuations of Asian aeolian deposits since the late Oligocene. Earth Sci. Rev. 200, 102963. https://doi.org/10.1016/j.earscirev.2019.102963.

Sun, Y., Clemens, S.C., Guo, F., Liu, X., Wang, Y., Yan, Y., Liang, L., 2021. High-sedimentation-rate loess records: a new window into understanding orbital- and millennial-scale monsoon variability. Earth Sci. Rev. 220, 103731. https://doi.org/10.1016/j.earscirev.2021.103731.

Tang, C., Yang, H., Pancost, R.D., Griffiths, M.L., Xiao, G., Dang, X., Xie, S., 2017. Tropical and high latitude forcing of enhanced megadroughts in Northern China during the last four terminations. Earth Planet. Sci. Lett. 479, 98–107. https://doi.org/10.1016/j.epsl.2017.09.012.

Tian, S., Dai, G., Yin, Q., Meng, X., Zhang, Z., Zhu, Z., Xiao, G., 2022. Spatial differences in East Asian climate transition at ~260 ka and their links to ENSO. Quat. Sci. Rev. 296, 107805. https://doi.org/10.1016/j.quascirev.2022.107805.

Wagner, B., Vogel, H., Francke, A., Friedrich, T., Donders, T., Lacey, J.H., Leng, M.J., Regattieri, E., Sadori, L., Wilke, T., Zanchetta, G., Albrecht, C., Bertini, A., Combourieu-Nebout, N., Cvetkoska, A., Giaccio, B., Grazhdani, A., Hauffe, T., Holtvoeth, J., Joannin, S., Jovanovska, E., Just, J., Kouli, K., Kousis, I., Koutsodendris, A., Krastel, S., Lagos, M., Leicher, N., Levkov, Z., Lindhorst, K., Masi, A., Melles, M., Mercuri, A.M., Nomade, S., Nowaczyk, N., Panagiotopoulos, K., Peyron, O., Reed, J.M., Sagnotti, L., Sinopoli, G., Stelbrink, B., Sulpizio, R., Timmermann, A., Tofilovska, S., Torri, P., Wagner-Cremer, F., Wonik, T., Zhang, X., 2019. Mediterranean winter rainfall in phase with African monsoons during the past 1.36 million years. Nature 573, 256–260. https://doi.org/10.1038/s41586-019-1529-0.

Williams, D.F., Peck, J., Karabanov, E.B., Prokopenko, A.A., Kravchinsky, V., King, J., Kuzmin, M.I., 1997. Lake Baikal record of continental climate response to orbital insolation during the past 5 million years. Science 278, 1114–1117. https://doi.org/10.1126/science.278.5340.1114.

Winckler, G., Anderson, R.F., Fleisher, M.Q., McGee, D., Mahowald, N., 2008. Covariant glacial-interglacial dust fluxes in the equatorial Pacific and Antarctica. Science 320, 93–96. https://doi.org/10.1126/science.1150595.

Xiao, J.L., Porter, S.C., An, Z.S., Kumai, H., Yoshikawa, S., 1995. Grain size of quartz as an indicator of winter monsoon strength on the Loess Plateau of Central China during the last 130,000 yr. Quat. Res. 43, 22–29. https://doi.org/10.1006/qres.1995.1003.

Xiao, G., Zong, K., Li, G., Hu, Z., Dupont-Nivet, G., Peng, S., Zhang, K., 2012. Spatial and glacial-interglacial variations in provenance of the Chinese Loess Plateau. Geophys. Res. Lett. 39, L20715. https://doi.org/10.1029/2012GL053304.

Xiao, G., Dai, G., Tian, S., Peng, S., Li, L., Meng, X., Yin, Q., 2023. Periodic variations of alpine glaciation and desertification of the NE Tibetan Plateau: evidence from the loess-paleosol sequences in the Menyuan Basin. Glob. Planet. Chang. 226, 104160. https://doi.org/10.1016/j.gloplacha.2023.104160.

Yang, S., Ding, Z., 2014. A 249 kyr stack of eight loess grain size records from northern China documenting millennial-scale climate variability. Geochem. Geophys. Geosyst. 15, 798–814. https://doi.org/10.1002/2013GC005113.

Zhang, H., Nie, J., Liu, X., Pullen, A., Li, G., Peng, W., Zhang, H., 2021. Spatially variable provenance of the Chinese Loess Plateau. Geology 49, 1155–1159. https://doi.org/10.1130/G48867.1.

Zhang, H., Lu, H., He, J., Xie, W., Wang, H., Zhang, H., Breecker, D., Bird, A., Stevens, T., Nie, J., Li, G., 2022a. Large-number detrital zircon U-Pb ages reveal global cooling caused the formation of the Chinese Loess Plateau during late Miocene. Sci. Adv. 8, eabq2007. https://doi.org/10.1126/sciadv.abq2007.

Zhang, J., Hao, Q., Li, S.-H., 2022b. An absolutely dated record of climate change over the last three glacial-interglacial cycles from Chinese loess deposits. Geology 50, 1116–1120. https://doi.org/10.1130/G50125.1.

Zhao, Y., Tzedakis, P.C., Li, Q., Qin, F., Cui, Q., Liang, C., Birks, H.J.B., Liu, Y., Zhang, Z., Ge, J., Zhao, H., Felde, V.A., Deng, C., Cai, M., Li, H., Ren, W., Wei, H., Yang, H., Zhang, J., Yu, Z., Guo, Z., 2020. Evolution of vegetation and climate variability on the Tibetan Plateau over the past 1.74 million years. Sci. Adv. 6, eaay6193. https://doi.org/10.1126/sciadv.aay6193.

Zhou, L.P., Shackleton, N.J., 1999. Misleading positions of geomagnetic reversal boundaries in Eurasian loess and implications for correlation between continental and marine sedimentary sequences. Earth Planet. Sci. Lett. 168, 117–130. https://doi.org/10.1016/S0012-821X(99)00052-7.

Zhou, W., Beck, J.W., Kong, X., An, Z., Qiang, X., Wu, Z., Xian, F., Ao, H., 2014. Timing of the Brunhes-Matuyama magnetic polarity reversal in Chinese loess using ^{10}Be. Geology 42, 467–470. https://doi.org/10.1130/G35443.1.

Zhou, G., Li, L., Xiao, G., Yan, L., Pearson, D.G., Hao, Q., Wu, Y., 2022. New constraints on the source of loess from U/Th-Pb geochronology of detrital multi-minerals. Geology 50, 1156–1160. https://doi.org/10.1130/G50075.1.

Zhou, W., Kong, X., Paterson, G.A., Sun, Y., Wu, Y., Ao, H., Xian, F., Du, Y., Tang, L., Zhou, J., Shi, Z., Jull, A.J.T., Zhao, G., An, Z., 2023. Eccentricity-paced geomagnetic field and monsoon rainfall variations over the last 870 kyr. Proc. Natl. Acad. Sci. USA, e2211495120. https://doi.org/10.1073/pnas.2211495120.

Zhu, R., Guo, B., Ding, Z., Guo, Z., Kazansky, A., Matasova, G., 2000. Gauss-Matuyama polarity transition obtained from a loess section at Weinan, North Central China. Chin. J. Geophys. 43, 621–634. https://doi.org/10.1002/cjg2.81 (in Chinese with English abstract).